crystals

MDPI

*Article*

# Facile Green Synthesis of Silver Nanoparticles Using Aqueous Leaf Extract of *Origanum majorana* with Potential Bioactivity against Multidrug Resistant Bacterial Strains

**Mohamed Taha Yassin *, Ashraf Abdel-Fattah Mostafa, Abdulaziz Abdulrahman Al-Askar and Fatimah O. Al-Otibi**

Botany and Microbiology Department, College of Science, King Saud University, P.O. 2455, Riyadh 11451, Saudi Arabia; asali@ksu.edu.sa (A.A.-F.M.); aalaskara@ksu.edu.sa (A.A.A.-A.); falotibi@ksu.edu.sa (F.O.A.-O.)

* Correspondence: myassin2.c@ksu.edu.sa

**Abstract:** The high prevalence of nosocomial bacterial resistance contributes to significant mortality and morbidity around the world; thus, finding novel antibacterial agents is of vital concern. Accordingly, the present study attempted to synthesize silver nanoparticles (AgNPs) using a green approach. Aqueous leaf extract of *Origanum majorana* was used to synthesize AgNPs and the antibacterial efficiency against multidrug resistant bacterial strains was detected. Characterization of the biogenic AgNPs was performed using ultraviolet-visible spectrophotometry (UV-Vis), transmission electron microscopy (TEM), energy dispersive X-ray spectroscopy (EDX), Fourier transform infrared spectroscopy (FT-IR) analysis, and X-ray diffraction analysis (XRD). The disc diffusion method was used to detect the antibacterial activity of AgNPs against three nosocomial multidrug-resistant strains. Preliminary UV-Vis analysis revealed the biosynthesis of AgNPs due to peak formation at 374 nm, corresponding to the surface plasmon resonance (SPR) of biogenic AgNPs. TEM micrographs detected the synthesis of small AgNPs with an average particle size of 26.63 nm. EDX analysis revealed the presence of the following elements: oxygen (3.69%), carbon (2.93%), aluminum (1.29), silicon (2.83%), chloride (17.89%), and silver (71.37%). Furthermore, XRD analysis revealed the presence of diffraction peaks at 2 theta (θ) degrees of 38.18°, 44.36°, 64.35°, and 77.54°, assigned to the planes of silver crystals (111), (200), (220), and (311), respectively. Collectively, these findings affirm the synthesis of biogenic AgNPs with potential physicochemical characteristics. The antimicrobial efficiency of the biogenic AgNPs indicated that *Klebsiella pneumoniae* strain was the most susceptible strain at concentrations of 50 and 100 µg/disk, with inhibitory zones of 21.57 and 24.56 mm, respectively. The minimum inhibitory concentration (MIC) of AgNPs against *Klebsiella pneumoniae* strain was found to be 10 µg/mL, while the minimum bactericidal concentration (MBC) was found to be 20 µg/mL. In conclusion, aqueous leaf extract of *O. majorana* mediated synthesis of small sized AgNPs, with potential antimicrobial effectiveness against multidrug-resistant bacterial pathogens.

**Keywords:** *Origanum majorana*; silver nanoparticles; nosocomial infections; bacterial resistance



**Citation:** Yassin, M.T.; Mostafa, A.A.-F.; Al-Askar, A.A.; Al-Otibi, F.O. Facile Green Synthesis of Silver Nanoparticles Using Aqueous Leaf Extract of *Origanum majorana* with Potential Bioactivity against Multidrug Resistant Bacterial Strains. *Crystals* **2022**, *12*, 603. https://doi.org/10.3390/cryst12050603

Academic Editor: Anatoliy V. Glushchenko

Received: 27 March 2022
Accepted: 23 April 2022
Published: 25 April 2022



## 1. Introduction

Antimicrobial resistance is a global health concern that has resulted in a high number of deaths worldwide [1]. In this setting, antibiotic overuse has resulted in significant prevalence of multidrug-resistant bacterial strains [2]. Antimicrobial-resistant bacterial strains cause serious infections which can resulted in a number of harmful consequences, including higher death and morbidity rates, longer hospital stays, and financial losses [3]. In this context, methicillin-resistant *Staphylococcus aureus* (MRSA) strains, which are resistant to all known β-lactam antibiotics, as well as other clinical MRSA strains that are resistant to linezolid, vancomycin, and daptomycin have made *S. aureus* a dominant cause of morbidity and death globally [4]. These bacteria have been reported to cause serious

infections such as osteomyelitis, endocarditis, pneumonia, and sepsis when transmitted to the human bloodstream [5]. *Klebsiella pneumonia* is the second-most prevalent gram negative bacterium, causing invasive infections such as pneumonia and meningitis [6]. *K. pneumoniae* is an opportunistic bacterial strain that belongs to the Enterobacteriaceae family; it is linked to nosocomial infections such as urinary tract, respiratory, sepsis, and pneumonia infections [7]. This bacterium can build biofilms on congenital medical equipment, resulting in serious nosocomial infection [8]. *Acinetobacter baumannii* is another gram negative and highly resistant bacterial strain responsible for number of hospitalized bacterial infections, such as pneumonia, respiratory infections, and urinary tract infection, resulting in high mortality rate, especially in intensive care units [9].

Nanotechnology is one potential way to overcome the high incidence of multidrug resistant bacterial strains [10]. In this context, nanoparticles are believed to be able to combat the common resistance mechanisms of bacteria to antibacterial agents, such as enzyme inactivation, reduced cell permeability, efflux pumps overexpression, and disruption of drug target site in order to escape from different antibacterial agents [11]. Moreover, nanoparticles utilize a variety of antimicrobial mechanisms including disrupting microbial membrane integrity and generating reactive oxygen species (ROS), which inhibits protein and RNA synthesis [12]. Furthermore, nanoparticles pose featured physicochemical and biological characteristics such as antitumor, anti-inflammatory, and antimicrobial proficiency [13]. Recently, AgNPs have gained a great deal of consideration due to their distinctive antimicrobial characteristics [14]. Silver nanomaterials are the most frequently used medical nanoparticles, with applications in diagnostics, coatings, and sensors [15]. Furthermore, AgNPs are reported to be a promising tool for the bioformulation of new antimicrobial agents, fabrication of drug delivery formulations, and development of diagnostic and detection platforms [16]. In addition, AgNPs have been fabricated according to variety of factors including pH, temperature, media, solvents type, preparation method, and $AgNO_3$ concentration [17]. AgNP efficacy is reported to depend on physical features including shapes, sizes and coating agents [18]. Bacterial cells are prokaryotic and less complicated, though incapable of combating AgNP toxicity [19]. AgNPs inhibit bacterial growth by entering the cell and hindering its vital processes at the cellular and subcellular levels [20]. The chemical method is a simple method of AgNP synthesis that results in high yield production [21]. In contrast, the main disadvantages of the chemical approach to AgNP synthesis is the high cost of synthesis and the additional procedures required for the prevention of particle aggregation [22]. Furthermore, chemically fabricated nanomaterials discharge hazardous byproducts to the environment [23]. In addition, adopting a chemical technique for AgNP synthesis necessitates the use of hazardous reducing and capping agents, resulting in toxic chemical adsorption on nanoparticles, which has a negative impact during application [24]. On the other hand, less hazardous stabilizing and reducing agents have been used for green biosynthesis of nanomaterials, especially using plant extracts [25]. Moreover, the reaction procedure for the production of biogenic nanomaterials using plant extracts occurs in natural circumstances without being constrained by severe or strict reaction conditions [26]. The lower cytoxicity of these nanoparticles is another advantage of plant extract-mediated green synthesized nanomaterials [27]. Green synthesized nanoparticles are regarded as cost-effective, eco-friendly, and safe alternative for antimicrobial applications [28]. Biogenic AgNPs exhibit higher antibacterial efficacy against human pathogens than chemically-produced ones, with MIC ranges of (0.06–0.25 g/mL) and (2.5–5.0 g/mL) respectively, according to a previous study [29]. Green synthesized nanomaterials exhibit higher antifungal effectiveness compared to chemically synthesized nanomaterials [30]. The essential oils of *Origanum* species such as *O. vulgare* (oregano) and *O. majorana* (marjoram) have been shown to be rich in phenolic compounds, which have been found to be effective reducing agents of silver nitrate for the synthesis of silver nanoparticles [31,32]. A previous study reported that *Origanum vulgare* aqueous leaf extract mediated biosynthesis of green AgNPs with average particle size of 136 $\pm$ 10.09 nm, demonstrating antibacterial efficiency against *Escherichia coli*, *Aeromonas hydrophilla*, *Salmonella paratyphi*, and *Shigella*

*dysenteriae* strains with inhibition zone diameters higher than 10 mm [33]. Another study published in 2018 by Shaik et al. confirmed the green synthesis of AgNPs using *Origanum vulgare* aqueous leaf extract as a reducing agent and reported antibacterial efficacy against Gram negative and Gram positive bacterial strains with inhibition zones ranging from 12 to 19 mm in diameter [34]. Previous studies evaluated the antibacterial efficacy of green AgNPs synthesized using *O. vulgare* leaf extract against various bacterial strains without investigating the antibiotic resistance patterns of these bacterial pathogens. Furthermore, previous studies focused on the green synthesis of AgNPs utilizing *O. vulgare* aqueous leaf extract; thus, the current study was conducted to investigate the ability of the other *Origanum* species, namely, *O. majorana*, to synthesize AgNPs. Moreover, the resistance patterns of the tested bacterial strains to different antibiotics were detected to ensure their resistance and then the antibacterial effectiveness of the green AgNPs was investigated against the tested multidrug-resistant bacterial strains.

## 2. Materials and Methods

### 2.1. Preparation of Plant Extracts

*Origanum majorana* leaves were collected from a local market in Riyadh, Saudi Arabia. The collected plant materials were first identified by the Herbarium of the Botany and Microbiology Department. The leaves of *Origanum majorana* were washed twice with tap water then twice with distilled water. After complete dryness was reached, the plant parts were ground using a mechanical mortar to obtain a homogenous powder. Fifty grams of the powdered plant materials were submerged in 500 mL flasks containing 200 mL of deionized water and heated over a hot plate for 30 min at 50 °C. The flasks were incubated at 25 °C for 24 h over a magnetic stirrer, then the extracts were filtered using Whatman 1 filter paper grade 1. The aqueous extracts of *Origanum majorana* were stored in the refrigerator at 4 °C for further use [35,36].

### 2.2. Green Synthesis of Silver Nanoparticles (AgNPs)

Synthesis of AgNPs was achieved by adding 10 mL of the previously prepared aqueous leaf extract of *O. majorana* to 90 mL of silver nitrate ($AgNO_3$) solution (1 mM). After heating the mixture over a magnetic stirrer for 1 h at 70 °C, the color of the $AgNO_3$ solution changed from colorless to a dark brown color, indicating AgNPs synthesis. The biogenic AgNPs were harvested by centrifugation of the tubes containing the reduced silver nanomaterials at 10,000 rpm for 10 min. Subsequently, the supernatants were discarded and the precipitate was collected. The collected silver precipitates were washed thrice using distilled water and dried using an oven at 80 °C. The dried silver nanomaterials were used for further analysis and characterization [37].

### 2.3. Characterization of AgNPs

#### 2.3.1. UV Optical Spectroscopy

The biosynthesized silver nanomaterials were first dispersed in distilled $H_2O$, then the absorption was measured in the wavelength range of 200–800 nm using a UV–VIS-NIR spectrophotometer (UV-1601, Shimadzu, Japan). Distilled water was used as a blank.

#### 2.3.2. Transmission Electron Microscopy (TEM) Analysis

The synthesized nanomaterials were first washed three times with deionized water. The samples were placed over a carbon-coated copper grid, detached, and dried before examination. A TEM assay was carried out using a Transmission Electron Microscope (JEOL, JEM1011, Tokyo, Japan) at the Electron Microscope Unit of the College of Science at King Saud University. The TEM assay detected the morphological features and particle size distribution of AgNPs through the generation of high-resolution two dimensional images at 100 kv voltage.

#### 2.3.3. Energy Dispersive X-ray (EDX) Analysis

Elemental analysis of AgNPs was performed using a Scanning Electron Microscope (SEM) integrated with an Energy Dispersive X-ray (EDX) analyzer (JEOL, JSM-6380 LA, Tokyo, Japan).

#### 2.3.4. FTIR (Fourier Transform Infrared) Analysis

FTIR spectroscopy was used to analyze the surface chemistry of the prepared silver nanomaterials. The functional groups attached to the surface of the nanoparticles were detected in the range of 400–4000 $cm^{-1}$, depending on the infrared absorption frequency. Sample preparation was performed by dispersing AgNPs in a dry KBr matrix which was then compacted to form a transparent disc. A KBr pellet was used as a standard.

#### 2.3.5. XRD Analysis

A Shimadzu XRD model 6000 diffractometer (Shimadzu, Columbia, United States) fitted with a graphite monochromator was utilized to acquire X-ray powder diffraction (XRD) patterns using Cu-K radiation. Step-scanning software with 0.02 per step and an acquisition duration of 5 s per step at 2-theta was used to measure XRD on a film of the biosynthesized silver nanoparticles. The crystalline phases were identified using Joint Committee on Powder Diffraction Standards (JCPDS).

#### 2.3.6. Zeta Potential Analysis

The zeta potential analysis of the biosynthesized silver nanomaterials was characterized using a zeta sizer instrument (Malvern Instruments Ltd.; zs90, Worcestershire, UK) based on photon correlation spectroscopy.

### *2.4. Bacterial Strains used in the Study*

Three nosocomial bacterial strains were tested for susceptibility to the silver nanoparticles: methicillin-resistant *Staphylococcus aureus* (ATCC 33592), *Klebsiella pneumoniae* (ATCC 700603), and *Acinetobacter baumannii* (ATCC 43498). The bacterial isolates were subcultured over Mueller–Hinton agar (MHA) incubated for 48 h at 35 °C to attain fresh inoculums.

### *2.5. Antibiotic Susceptibility Testing*

For the preparation of bacterial suspension, fresh bacterial colonies were immersed in 0.85% sterile saline solution and the turbidity of the bacterial suspension was adjusted using 0.5 McFarland standard to achieve a viable cell count of $1.0 \times 10^8$ cfu/mL. Freshly prepared MHA plates were inoculated with 0.5 mL of the prepared bacterial suspension. Seven different antibiotics were used to investigate the resistance profile of the concerned bacterial strains to these antibiotics. Cefaclor (30 µg), cefixime (5 µg), cefatziodime (30 µg), ceftriaxone (30 µg), cefotaxime (30 µg), trimethoprim + sulfamethoxazole (25 µg), and norfloxacin (10 µg) antibiotic disks were purchased from MASTDISCS (Mast Group Ltd., Mast House, Merseyside, U.K.). These antibiotic disks were placed over the inoculated MHA plates, incubated at 37 °C for 24 h, and the inhibition zones were measured by Vernier caliper. The resistance patterns of different bacterial strains were interpreted as demonstrated by the clinical and laboratory standards institute [38].

### *2.6. Antibacterial Efficiency of AgNPs*

The biogenic AgNPs were investigated for their antibacterial effectiveness against the concerned bacterial strains using a disk diffusion assay. The powdered silver nanoparticles were dissolved in methanol and sonicated to ensure complete dissolution of the biogenic nanomaterials. Afterwards, sterile filter paper disks 8 mm in diameter were impregnated with 50 and 100 µg of the biogenic nanomaterials. Freshly prepared MHA plates were seeded with the bacterial suspension as mentioned above. Norfloxacin discs (10 µg) were utilized as a positive control, while disks impregnated with methanol only were used as a negative control. The silver nanoparticle-loaded disks were placed over the MHA

plates seeded with the bacterial slurry and the plates were refrigerated for two hours to allow the nanoparticles to diffuse. Finally, the plates were incubated at 37 °C for 24 h and the suppressive zones were measured by Vernier caliper. A broth microdilution assay was used to determine the MIC of the *O. majorana* silver nanoparticles against different bacterial strains using 96-well microtitre plates, as stated in a prior study [39]. The MBC was determined by streaking MIC wells into freshly prepared MHA plates and checking for bacterial growth. The lowest concentration of AgNPs that reported no bacterial growth was recorded as MBC [40].

### *2.7. Statistical Analysis*

Statistical analysis of data was performed by GraphPad Prism 5.0 (GraphPad Software, Inc., La Jolla, CA, USA) using one way analysis of variance. The data were presented as a mean of triplicates ± standard error, and the experimentations were done in three replicates.

## 3. Results and Discussion

### *3.1. UV–Vis Spectral Analysis*

The change in color of $AgNO_3$ from colorless to dark brown first revealed AgNP synthesis, as seen in Figure 1. After the dark brown color revealed AgNP synthesis in this condition, color intensity varied depending on AgNP size and intensity, showing that the color was due to excitation of AgNPs surface plasmon resonance. UV-Vis spectroscopy was achieved to affirm AgNP synthesis utilizing aqueous leaf extract of *O. majorana*. The UV-Vis spectrum revealed the formation of three absorption peaks at 242, 345 and 374 nm, as seen in Figure 2. The broad peak observed at 242 nm in the UV spectrum of the AgNPs can be attributed to the biomolecules of the aqueous leaf extract of *O. majorana*, as stated by a prior study [41]. The peaks detected at 283 and 322 nm in the UV spectrum of *O. majorana* were shifted to 345 and 374 nm in the spectrum of the biogenic AgNPs, indicating the surface plasmon resonance (SPR) of the biosynthesized AgNPs [42]. Our results are in accordance with those of a prior study which stated the formation of a UV-absorption band at 374 nm as indicating AgNP formation [42,43].

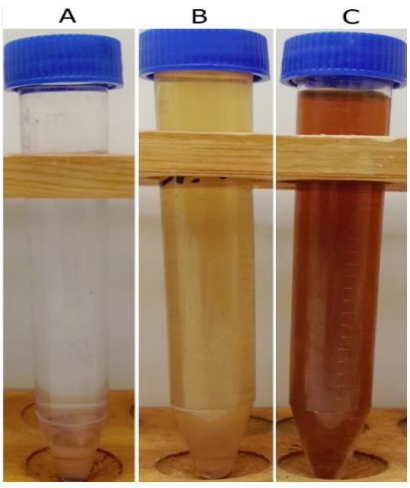


**Figure 1.** Change in the color of silver nitrate solution after addition of *Origanum majorana* aqueous leaf extract. (**A**): colorless silver nitrate solution; (**B**): *Origanum majorana* aqueous leaf extract; (**C**): dark brown color indicates formation of silver nanoparticles.

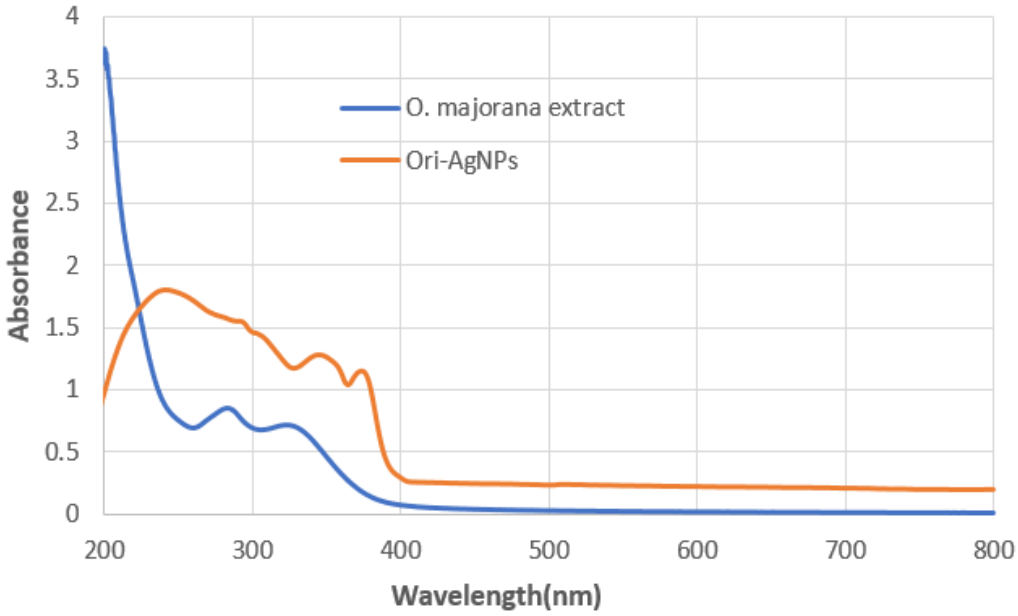


**Figure 2.** UV-vis spectrum of both *O. majorana* extract and the biogenic AgNPs.

### *3.2. TEM Analysis of the Biosynthesized Silver Nanoparticles*

Transmission electron microscope (TEM) analysis has been reported as the most accurate technique for the determination of AgNP size [44,45]. Electron micrographs of AgNPs showed that these nanomaterials were spherical in shape, polydispersed, and that their average size diameter ranged from 10–60 nm, as seen in Figure 3. Moreover, Figure 4 shows the AgNP size distribution histogram, which reveals that AgNP size was within permissible limits, with an average particle size of 26.63 nm. The biogenic silver nanoparticles were smaller than those described in a recent work in which *Phyllanthus emblica* fruit extract promoted green production of silver nanoparticles with an average diameter of 39.1 nm [46]. Larger sizes of green synthesized silver nanoparticles using fresh *Arbutus unedo* leaf extract have been reported, with typical size diameters ranging from 40 to 58 nm [47]. Overall, prior results confirm that utilizing aqueous leaf extract of *O. majorana* to synthesize silver nanoparticles is an eco-friendly and high-efficiency approach, as demonstrated in our current investigation.

### *3.3. Edx Analysis of AgNPs*

Energy dispersive X-ray spectroscopy (EDX) analysis was implemented to detect the elemental mapping of the biogenic AgNPs. EDX analysis showed the presence of the following elements: oxygen (3.69%), carbon (2.93%), aluminum (1.29), silicon (2.83%), chloride (17.89%), and silver (71.37%), as seen in Figure 5. Moreover, an intense peak was observed at 2.98 keV, indicating the presence of silver (Ag), while the intense peak formed at 2.62 keV confirmed the presence of chloride (Cl). Aluminum (Al) and silicon (Si) elements were ascribed to the two additional peaks found at 1.486 and 1.739 keV, respectively. Our findings were in accordance with those of Okaiyeto et al., 2019, who detected the elemental composition of AgNPs synthesized using aqueous leaf extract of *Oedera genistifolia*, showing the presence of silver and chloride elements [48]. Furthermore, *Benincasa hispida* peel extract and *Momordica charantia* leaf extract mediated green synthesis of silver nanoparticles with the presence of chloride element according to EDX analysis, and these results were coincident with our findings [49,50]. Chlorine ($Cl^-$) ions are plentifully existent in plants, and play a dynamic role through photosynthesis and keeping overall homeostasis [51]. Collectively, different elements detected by EDX analysis, such as Si, Al, and Cl, were reported to act as capping agents of the biogenic AgNPs according to a previous study [52].

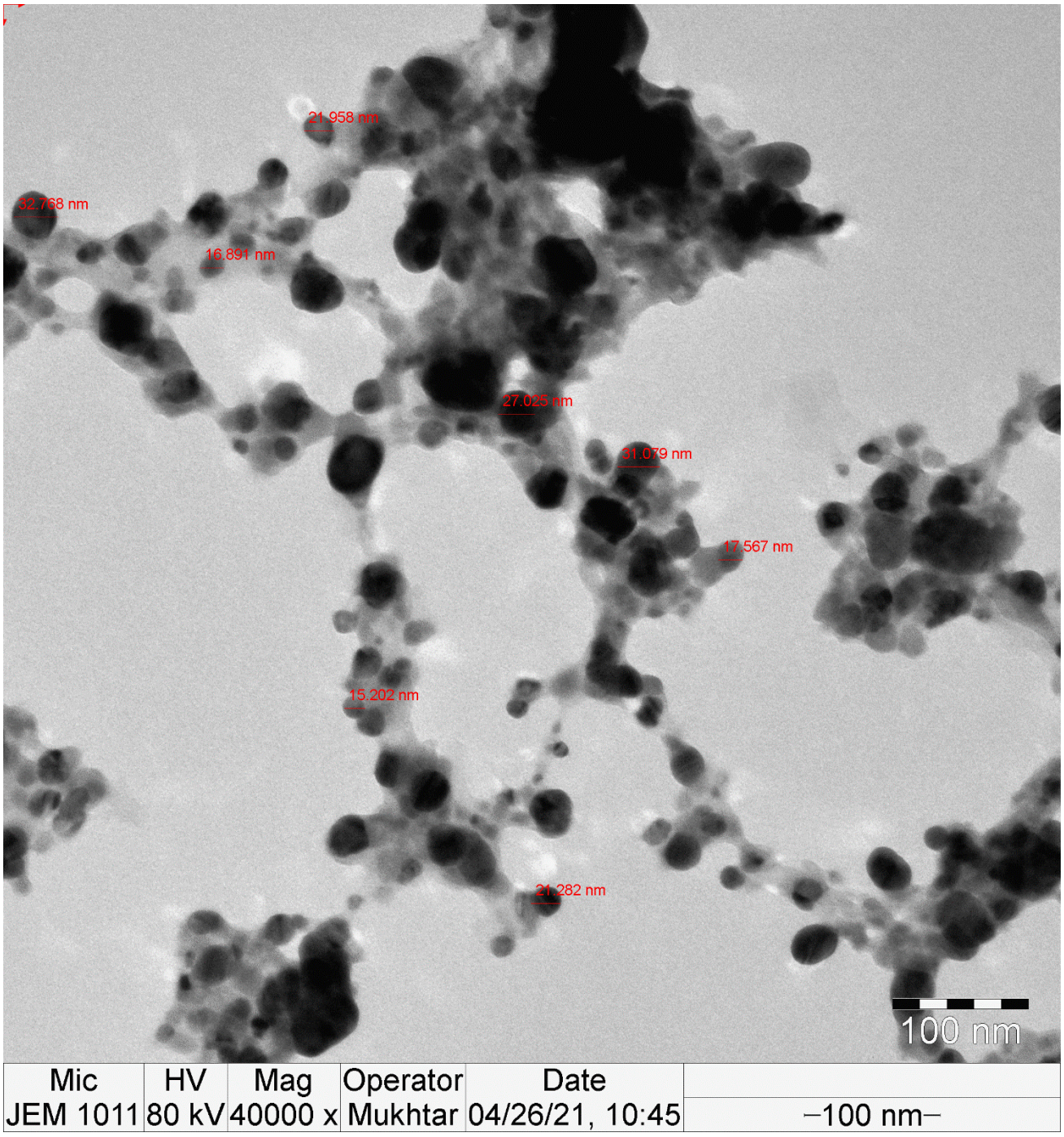


**Figure 3.** TEM micrograph of the biogenic AgNPs formulated using *O. majorana* extract.

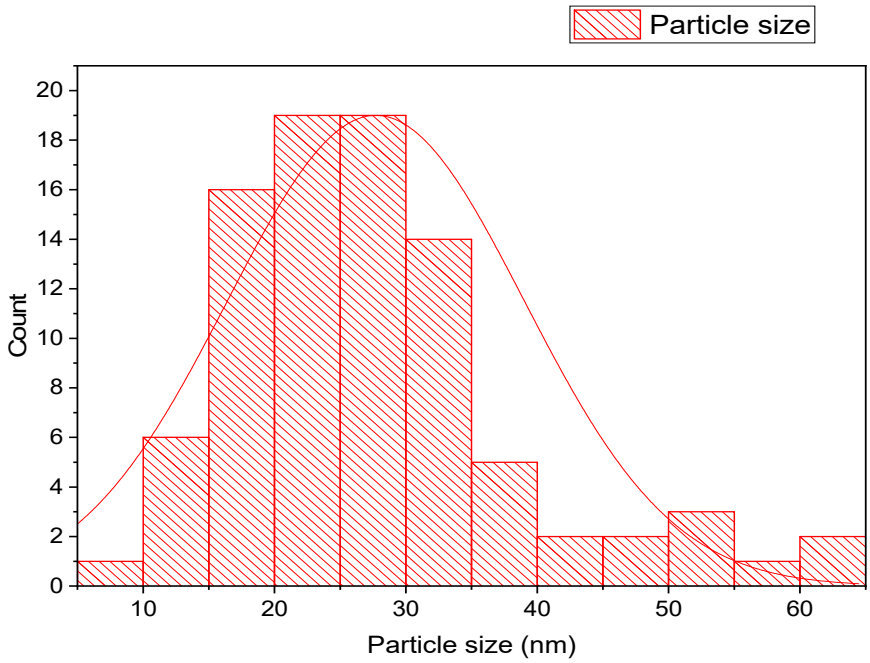


**Figure 4.** Particle size distribution histogram of AgNPs based on TEM micrographs.

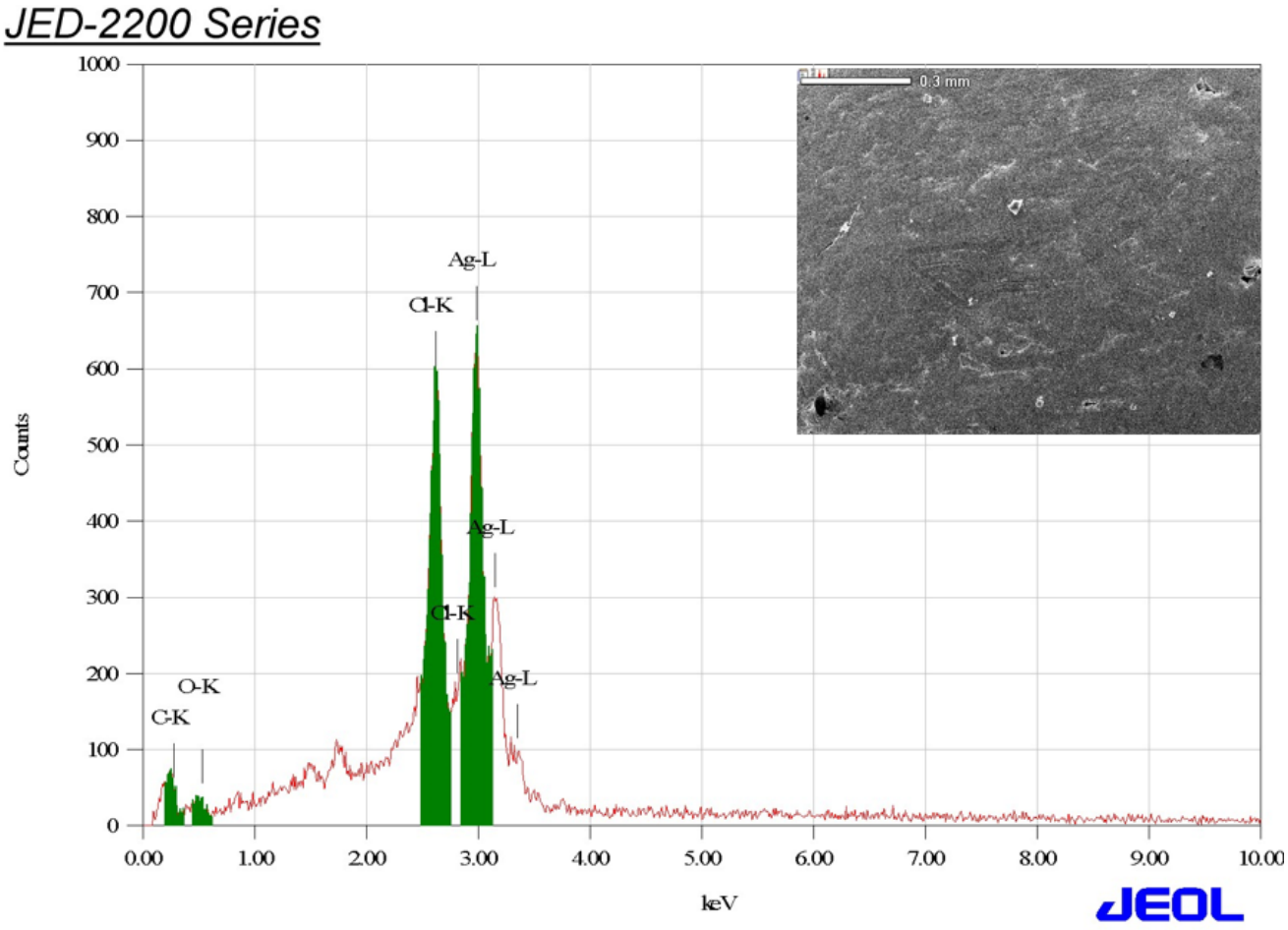


**Figure 5.** EDX spectrum and SEM graph of AgNPs fabricated using *O. majorana* extract.

### *3.4. Fourier Transform Infrared Spectroscopy (FT-IR) Analysis*

The distinct functional groups accountable for the reduction and stability of silver nanoparticles were investigated using FTIR analysis. FTIR analysis of aqueous leaf extract of *O. majorana* revealed the presence of vibrational frequencies at 3399.10, 2929.94, 1652.38, 1402.20, 1325.04, 1079.44, 880.06, 797.71, and 615.21 $cm^{-1}$, as seen in Figure 6. On the other hand, the biogenic AgNPs synthesized using *O. majorana* leaf extract showed vibrational frequencies at 3434.80, 1631.42, 1030.67, and 537.82 $cm^{-1}$, as seen in Figure 7. The broad bands at the vibrational frequencies of 3390 and 3434 $cm^{-1}$ of both plant extract and biogenic AgNPs were assigned to the presence of hydroxyl functional group, corresponding to phenolic compounds [53]. In this context, the hydroxyl functional groups detected in *O. majorana* extract were believed to be accountable for silver ions reduction to metal silver through alcoholic oxidation (R-OH) to form an aldehydic group (R=O) as demonstrated in the equation

$$2AgNO_3 + 2ROH \rightarrow 2Ag + 2RO + 2HNO_3 \quad (1)$$

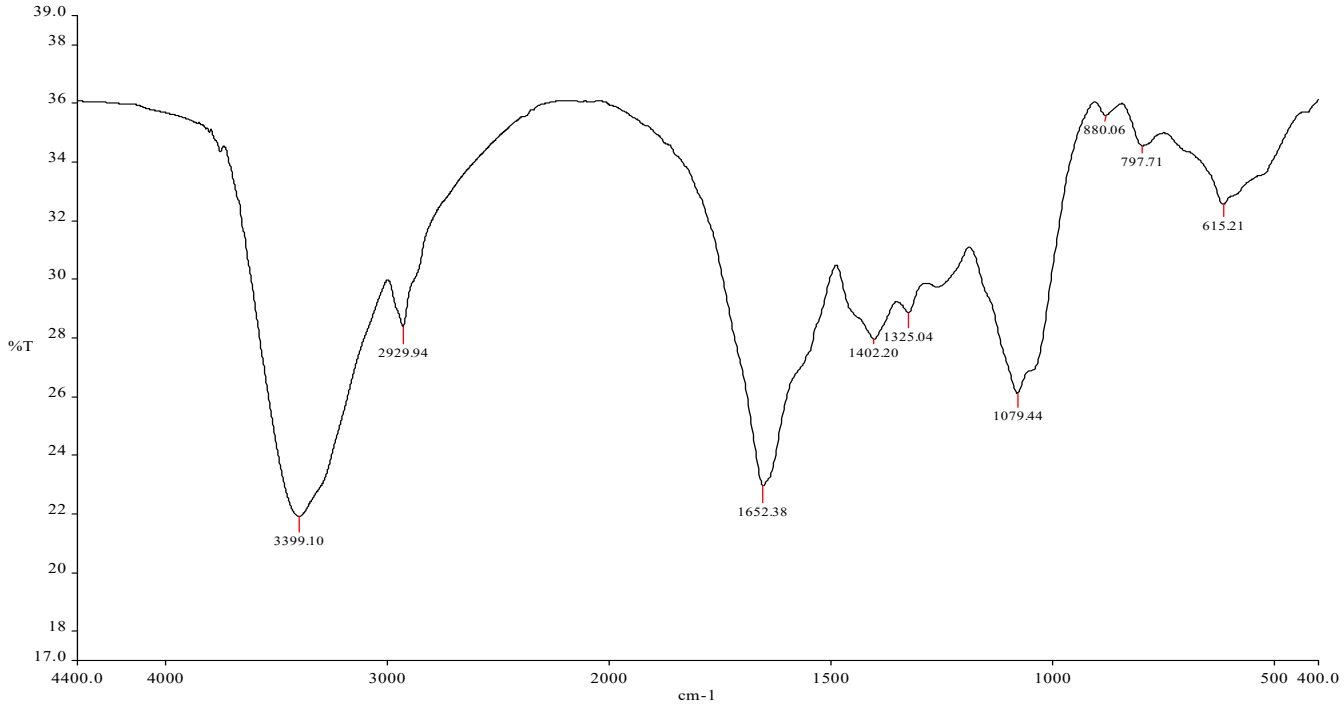


**Figure 6.** FTIR spectrum of *O. majorana* aqueous leaf extract.

This clearly demonstrates that the phenolic compounds in *O. majorana* extract functionalized as reducing and stabilizing agents during AgNPs synthesis [54]. The peak at 2929.94 $cm^{-1}$ was assigned to the presence of C-H stretching, corresponding to chlorophyll groups of *O. majorana* extract [55]. Moreover, the band observed at 1652.38 $cm^{-1}$ of *O. majorana* extract was shifted to a lower side at 1631.42 $cm^{-1}$, which was assigned to C=C aromatic vibration, as seen in Table 1 [56]. The peak detected at 1325.04 $cm^{-1}$ can be assigned to C-N stretching in proteins present in aqueous leaf extract of *O. majorana* [57]. Additionally, the broad band at 1079.44 $cm^{-1}$ of *O. majorana* extract was shifted to 1030 $cm^{-1}$ of biogenic AgNPs, indicating C–O stretching and confirming the adsorbance of flavonoid compounds on the surface of biosynthesized AgNPs [58]. Moreover, the observed band at 615.21 $cm^{-1}$ of plant extract was shifted to a lower number of 537.82 $cm^{-1}$, corresponding to C-I stretching of alkyl halides.

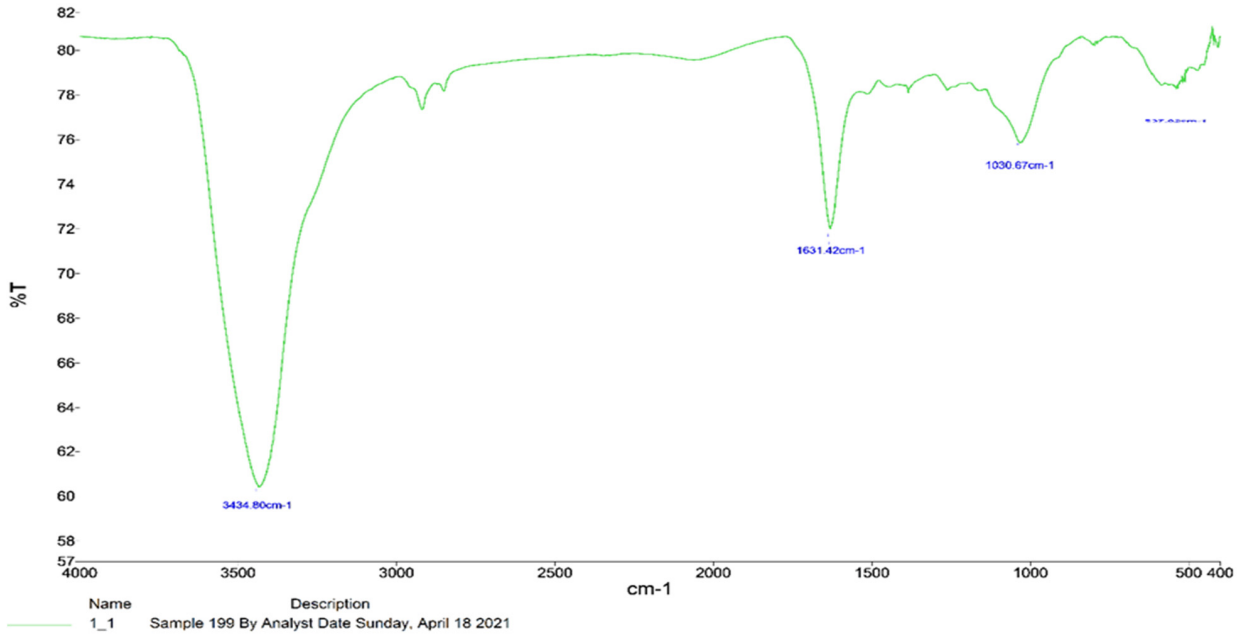


**Figure 7.** FTIR spectrum of AgNPs synthesized using aqueous extract of *Origanum majorana* extract.

**Table 1.** FTIR analysis of *O. majorana* extract and the biogenic AgNPs showing different functional groups.

| Tested Material | Absorption Peak ($cm^{-1}$) | Functional Groups | Molecular Motion |
|---|---|---|---|
| *O. majorana* extract | 3399.10 | Phenolics | O-H stretching |
| | 2929.94 | Alkane | C-H stretching |
| | 1652.38 | Conjugated alkene | C=C stretching |
| | 1402.20 | Sulfonyl chloride | S=O stretching |
| | 1325.04 | Aromatic amine | C-N stretching |
| | 1079.44 | Primary alcohol | C-O stretching |
| | 880.06 | Alkene | C=C bending |
| | 797.71 | Aromatic compound | C-H bending |
| | 615.21 | Halo compound | C-Br stretching |
| Ori-AgNPs | 3434.80 | Phenolics | O-H stretching |
| | 1631.42 | Cyclic alkenes | C=C stretching |
| | 1030.67 | Secondary alcohol | C–O stretching |
| | 537.82 | Halo compound | C-I stretching |

### *3.5. XRD Analysis*

The crystalline nature of AgNPs was examined using X-ray diffraction analysis (XRD) of the dried powder of AgNPs. The XRD pattern revealed the presence of four diffraction peaks at 2 theta (θ) degrees of 38.18°, 44.36°, 64.35°, and 77.54°. The diffraction peaks detected at 2 theta (θ) of 38.18°, 44.36°, 64.35°, and 77.54° corresponded to the planes of silver crystals (111), (200), (220), and (311), respectively, as seen in Figure 8. Accordingly, these findings confirmed the synthesis of face-centred cubic (*fcc*) and crystalline AgNPs [59]. Our findings were consistent with those of Al-Aboody 2019, who reported the formation of the *fcc* structure of AgNPs as a result of Bragg reflections at 28.0°, 32.4°, 46.4°, 54.9°, 57.7°, and 64.7°, which corresponded to the planes (111), (200), (220), (311), (222), and (400),

respectively, as stated by the Joint Committee on Powder Diffraction Standards (JCPDS), file No. 04-0783 [60].

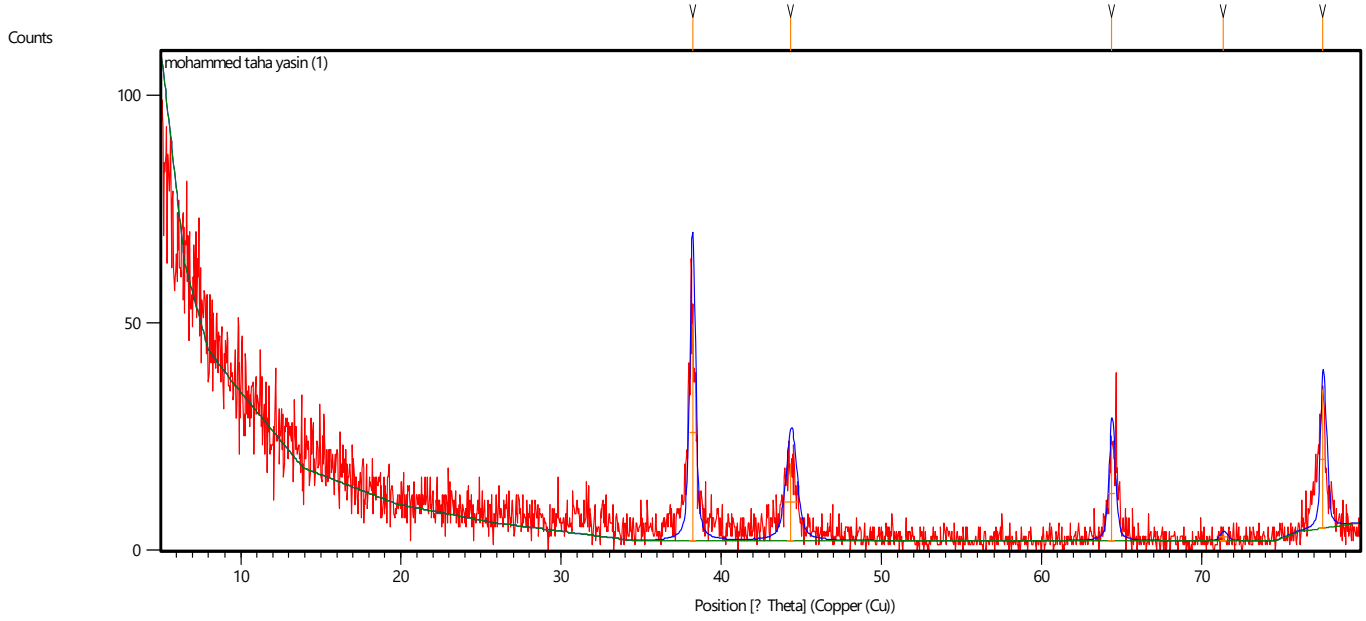


**Figure 8.** XRD pattern of the bio-inspired AgNPs.

### *3.6. Zeta Potential Analysis of the Biologically Synthesized Nanomaterials*

Zeta potential analysis was conducted to measure the surface charge of the biogenic AgNPs. In this regard the zeta potential of the synthesized silver nanoparticles was found to be −22.7 mV (Figure S1). A prior study indicated that the surface charge of AgNPs synthesized using *Symphytum officinale* leaf extract was −25.5 mV [61]. Moreover, the negative charge of the biogenic nanoparticles can be attributed to the capping effect of the biomolecules of *Origanum majorana* leaf extract [62]. The observed negative surface charge of the AgNPs indicated the electrostatic repulsion between them [63].

### *3.7. Antibiotic Sensitivity Testing*

Antibiotic susceptibility testing of *S. aureus*, *K. pneumonia* and *A. baumannii* strains to cefaclor, cefatziodime, cefixime, cefotaxime, ceftriaxone, norfloxacin, and trimethoprim +sulfamethoxazole (TS) antibiotics was conducted. *Acinetobacter baumannii* is an opportunistic organism that causes infections such as bacteremia, nosocomial pneumonia, ventilator-associated pneumonia, meningitis, catheter-associated urinary tract infection, central venous catheter-related bloodstream infection, and wound infection, especially in intensive care settings [64]. Furthermore, *A. baumannii* is the most predominant bacterial strain isolated from blood culture, the respiratory tract, and wound and urine samples [65]. The wide spectrum antibiotic treatment of intensive care unit patients contributes to the high occurrence of multi-drug resistance among *A. baumannii* strains [66]. Antibiotic resistance in *A. baumannii* strains is attributed to a number of mechanisms, including target modification, antibiotic inactivation, membrane permeability disruption, and a variety of other factors including outer membrane proteins, β-lactamases production, aminoglycoside-altering enzyme production, and efflux pump expression [67]. In this context, *Acinetobacter baumannii*, a gram negative bacterial strain, was found to be the most resistant strain to all tested antibiotics, whereas *K. pneumonia*, another gram negative strain, was found to be the most susceptible one, showing susceptibility to all antibiotics except ceftriaxone, as seen in Figure 9. Accordingly, β-lactamases are hydrolytic enzymes produced by *A. baumannii*, and contribute to its resistance to cephalosporins such as cefaclor, cefatziodime, cefixime, cefotaxime, and ceftriaxone antibiotics, as shown in the present study [68]. Our findings were in accordance with those of Hakyemez et al., 2013, who reported the 81.8% of isolated

nosocomial *A. baumannii* strains exhibited resistance to trimethoprim–sulfamethoxazole antibiotics [69]. Furthermore, *A. baumannii* strains isolated from ulcers, pus, sputum, and blood were shown to be resistant to the drug norfloxacin in 98.37% of total isolates [70]. On the other hand, *K. pneumoniae* strains showed resistance only to ceftriaxone drugs, coincident with Ahmadi et al., 2021, who reported that the clinical isolates of *K. pneumoniae* were highly resistant to ceftriaxone antibiotics [71]. On the contrary, MRSA strains exhibited resistance to cefaclor, cefatziodime, cefixime, cefotaxime, ceftriaxone, and trimethoprim+ sulfamethoxazole while showing sensitivity to norfloxacin antibiotics, as seen in Table 2. Parvin et al., 2021 confirmed the resistance of isolated MRSA strains to cefotaxime and cefixime antibiotics [72]. Additionally, all MRSA strains isolated from veterinary staff in six pet hospitals showed resistance to ceftriaxone antibiotics [73]. Antimicrobial susceptibility testing of MRSA strains isolated from nasal swaps of MBBS and BDS students at Kathmandu Medical College revealed that 100% of strains exhibited ceftriaxone resistance [74].

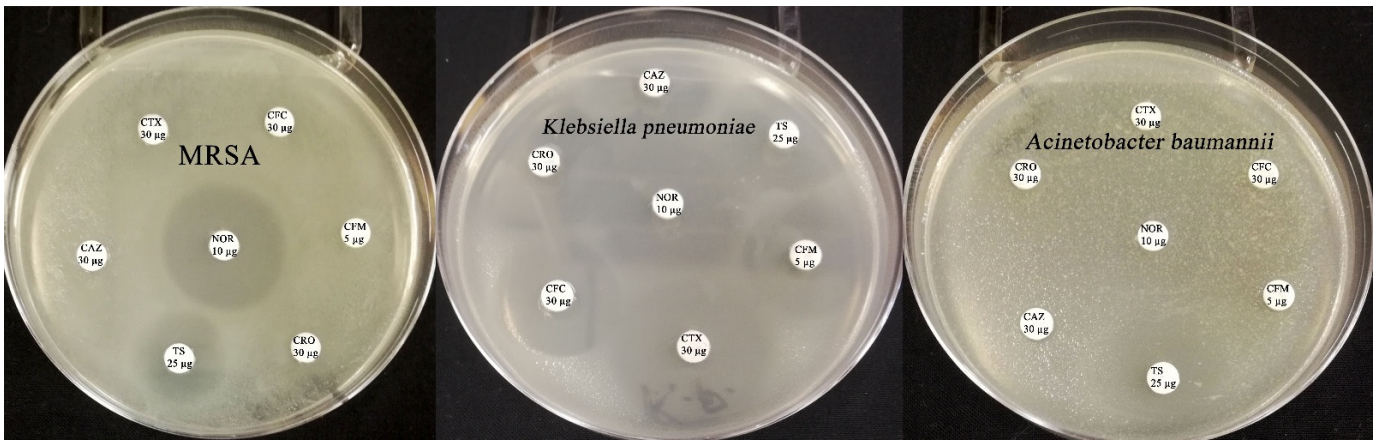


**Figure 9.** Antibacterial susceptibility testing of the tested bacterial strains against different antibiotics.

**Table 2.** Antibiotic susceptibility testing of the tested bacterial strains to different antibiotics.

| Antibiotics (µg/Disk) | Inhibition Zone Diameter (mm) | | | Interpretation Criteria | | |
|---|---|---|---|---|---|---|
| | MRSA | *A. baumannii* | *K. pneumonia* | R | I | S |
| Cefaclor (CFC) | 0.00 ± 0.00 (R) | 0.00 ± 0.00 (R) | 21.34 ± 0.12 (S) | ≤14 | 15–17 | ≥18 |
| Cefatziodime (CAZ) | 0.00± 0.00 (R) | 0.00 ± 0.00 (R) | 20.12 ± 0.26 (S) | ≤14 | 15–17 | ≥18 |
| Cefixime (CFM) | 0.00 ± 0.00 (R) | 0.00 ± 0.00 (R) | 22.14 ± 0.18 (S) | ≤15 | 16–18 | ≥19 |
| Cefotaxime (CTX) | 0.00 ± 0.00 (R) | 0.00 ± 0.00 (R) | 28.23 ± 0.34 (S) | ≤14 | 15–22 | ≥23 |
| Ceftriaxone (CRO) | 0.00 ± 0.00 (R) | 0.00 ± 0.00 (R) | 22.28 ± 0.21 (R) | ≤24 | 25–26 | ≥27 |
| Norfloxacin (NOR) | 20.14 ± 0.28 (S) | 9.80 ± 0.56 (R) | 25.12 ± 0.15 (S) | ≤12 | 13–16 | ≥17 |
| Trimethoprim + Sulfamethoxazole (TS) | 14.12 ± 0.31 (R) | 14.89 ± 0.14 (R) | 18.01 ± 0.09 (I) | ≤15 | 16–18 | ≥19 |

### *3.8. Screening of Antibacterial Efficiency of Green Synthesized Nanoparticles*

A disc diffusion assay was used to investigate the antibacterial efficiency of green synthesized nanomaterials against *S. aureus*, *K. pneumoniae* and *A. baumannii* strains, as seen in Figure 10. The *Klebsiella Pneumoniae* strain exhibited the highest sensitivity to *O. majorana* AgNPs at the concentrations of 50 and 100 µg/disk, recording inhibition zone diameters of 21.57 and 24.56 mm, respectively. These results were significantly higher than those of Hussein et al., 2019, who demonstrated the antibacterial efficiency of green AgNPs synthesized using ginger, onion, and sidr extracts and recorded suppressive zone diameters ranging from 8.33 ± 0.33 to 10.33 ± 0.33 mm [75]. Furthermore, the MRSA

strain showed high sensitivity to the biosynthesized AgNPs at the concentrations of 50 and 100 µg/disk, recording a suppressive zone diameter of 19.68 and 17.12 mm, respectively. These findings were in accordance with those of Ansari and Alzohairy 2018, who reported the antibacterial efficiency of AgNPs synthesized using seed extract of *Phoenix dactylifera* against MRSA strains at a concentration of 500 µg/mL, recording an inhibition zone diameter of 24 mm [76]. On the other hand, *A. baumannii* showed the lowest susceptibility to *O. majorana* AgNPs, showing inhibition zone diameters of 11.34 and 12.90 mm, respectively, which was significantly higher than that of control, as seen in Table 3. Our findings were consistent with those of Peiris et al., 2017, who reported that green synthesized silver nanomaterials exhibited antibacterial efficiency against *A. baumannii* with an inhibition zone diameter of 12 mm; furthermore, our findings were higher than those of the same study, because the antibacterial activity of biosynthesized AgNPs against MRSA in the current study was 19.68 mm, whereas it was 12.66 mm in the previous study [77]. Silver nanoparticles can continuously discharge silver ions, which could be a microbe-killing mechanism [78,79]. Furthermore, silver ions can cling to the cell wall and cytoplasmic membrane due to electrostatic attraction and affinity for sulfur proteins [80]. The attached ions can increase the permeability of the cytoplasmic membrane, causing the bacterial envelope to be disrupted [81]. Respiratory enzymes can be disabled once free silver ions are taken into cells, resulting in reactive oxygen species with no adenosine triphosphate synthesis [82]. In addition, the provocation of cell membrane rupture and deoxyribonucleic acid (DNA) alteration can be aided by reactive oxygen species [83]. Silver ions interact with sulfur and phosphorus, which are important components of DNA, causing problems with DNA replication, cell reproduction, and finally even microbial cell death [84]. Furthermore, silver ions can prevent protein production by denaturing ribosomes in the cytoplasm [85]. Smaller AgNPs, such as those found in the present study with a spherical shape and a tiny diameter of 26.63 nm, are more prone to silver release due to their increased surface area. Moreover, AgNPs have the capacity to penetrate bacterial cell walls and modify the structure of the cell membrane owing to their nanoscale size. Denaturation of the cytoplasmic membrane can cause organelle rupture and possibly cell lysis [86].

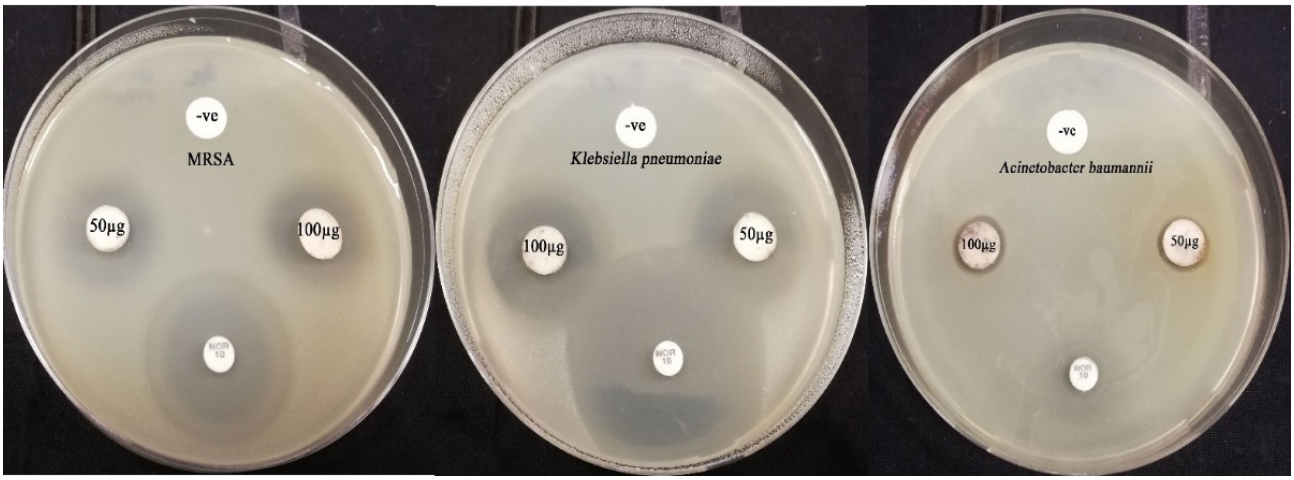


**Figure 10.** Antibacterial activity of AgNPs against the concerned bacterial pathogens.

The minimum inhibitory concentration was detected for *O. majorana* AgNPs against different bacterial pathogens. The MIC of the biogenic AgNPs against *K. pneumoniae* strain was 10µg/mL, while the MBC was found to be 20 µg/mL. The MIC value of *O. majorana* AgNPs was lower than that reported by Mortazavi-Derazkola et al., 2021, who evaluated the MIC of AgNPs synthesized utilizing *laeagnus angustifolia* bark extract and reported that the MIC value was 20µg/mL against *K. pneumoniae* [87]. The high efficiency of the AgNPs utilized in the current study compared to the previous study may be attributed

to their small nanoparticle size of 26.63 nm diameter; in the previously mentioned study, the particle size was 65–90 nm in diameter. Small particle size of biosynthesized AgNPs has previously been linked to antibacterial efficiency, as the nanoparticles' small diameter allows for high penetration of the bacterial cell wall and resulting cell membrane disruption, explaining the high antibacterial efficiency of the biogenic AgNPs in the current study [88].

**Table 3.** Antibacterial efficiency of AgNPs against different bacterial strains.

| Silver Nanoparticles | Inhibition Zone Diameter (mm) | | |
|---|---|---|---|
| | **MRSA** | ***A. baumannii*** | ***K. pneumonia*** |
| AgNPs (50 µg/disk) | 17.12 ± 0.12 | 11.34 ± 0.24 | 21.57 ± 0.21 |
| AgNPs (100 µg/disk) | 19.68 ± 0.42 | 12.90 ± 0.36 | 24.56 ± 0.11 |
| Norfloxacin (+ve control) | 20.45 ± 0.19 | 9.78 ± 0.16 | 36.84 ± 0.32 |
| -ve control | 0.00 ± 0.00 | 0.00 ± 0.00 | 0.00 ± 0.00 |
| MIC (µg/mL) | 20 | 40 | 10 |

## 4. Conclusions

Aqueous leaf extract of *O. majorana*-mediated green synthesis of AgNPs with potential physicochemical and antimicrobial properties and subsequent characterization of AgNPs confirmed that the produced particles were spherical in shape, with an average size diameter of 26.63 mm and a surface charge of −22.7 mV. The synthesized AgNPs exhibited potential antibacterial activity against the tested multidrug-resistant strains. Accordingly, these AgNPs could be a potential source for the production of highly efficient antimicrobial coatings in intensive care units and environmental surfaces in hospitals, preventing the spread of multidrug-resistant nosocomial bacterial infections.

**Supplementary Materials:** The following supporting information can be downloaded at: https://www.mdpi.com/article/10.3390/cryst12050603/s1, Figure S1: Zeta potential analysis of the synthesized silver nanoparticles.

**Author Contributions:** Conceptualization, M.T.Y. and A.A.A.-A.; methodology, M.T.Y.; software, M.T.Y.; validation, M.T.Y., A.A.A.-A. and F.O.A.-O.; formal analysis, A.A.A.-A., F.O.A.-O. and A.A.-F.M.; investigation, M.T.Y.; resources, A.A.A.-A.; data curation, M.T.Y.; writing—original draft preparation, M.T.Y.; writing—review and editing, M.T.Y., A.A.-F.M., A.A.A.-A. and F.O.A.-O.; visualization, A.A.-F.M.; supervision, A.A.A.-A., F.O.A.-O.; project administration, A.A.A.-A.; funding acquisition, A.A.-F.M. All authors have read and agreed to the published version of the manuscript.

**Funding:** The study was funded by the Researchers Supporting Project number (RSP-2021/362), King Saud University, Riyadh, Saudi Arabia.

**Data Availability Statement:** The datasets used and/or analyzed during the current study are available from the corresponding author on reasonable request.

**Acknowledgments:** The authors extend their appreciation to the Researchers Supporting Project number (RSP-2021/362), King Saud University, Riyadh, Saudi Arabia.

**Conflicts of Interest:** The authors declare that they have no conflict of interest.

## References

1. Dadgostar, P. Antimicrobial resistance: Implications and costs. *Infect. Drug Resist.* **2019**, *12*, 3903. [CrossRef] [PubMed]
2. Cerceo, E.; Deitelzweig, S.B.; Sherman, B.M.; Amin, A.N. Multidrug-resistant gram-negative bacterial infections in the hospital setting: Overview, implications for clinical practice, and emerging treatment options. *Microb. Drug Resist.* **2016**, *22*, 412–431. [CrossRef] [PubMed]
3. Pulingam, T.; Parumasivam, T.; Gazzali, A.M.; Sulaiman, A.M.; Chee, J.Y.; Lakshmanan, M.; Chin, C.F.; Sudesh, K. Antimicrobial resistance: Prevalence, Economic Burden, Mechanisms of Resistance and Strategies to Overcome. *Eur. J. Pharm. Sci.* **2021**, *170*, 106103. [CrossRef]

4. Lee, A.S.; De Lencastre, H.; Garau, J.; Kluytmans, J.; Malhotra-Kumar, S.; Peschel, A.; Harbarth, S. Methicillin-resistant Staphylococcus aureus. *Nat. Rev. Dis. Primers.* **2018**, *4*, 1188–1196. [CrossRef] [PubMed]
5. Lakhundi, S.; Zhang, K. Methicillin-resistant *Staphylococcus aureus*: Molecular characterization, evolution, and epidemiology. *Clin. Microbiol. Rev.* **2018**, *31*, e00020-18. [CrossRef]
6. Shi, Y.-F.; Wang, Y.-K.; Wang, Y.-H.; Liu, H.; Shi, X.-H.; Li, X.-J.; Wu, B.-Q. Metastatic infection caused by hypervirulent Klebsiella pneumonia and co-infection with Cryptococcus meningitis: A case report. *World J. Clin. Cases.* **2019**, *7*, 3812. [CrossRef]
7. Juhász, J.; Ligeti, B.; Gajdács, M.; Makra, N.; Ostorházi, E.; Farkas, F.B.; Stercz, B.; Tóth, Á.; Domokos, J.; Pongor, S.; et al. Colonization dynamics of multidrug-resistant Klebsiella pneumoniae are dictated by microbiota-cluster group behavior over individual antibiotic susceptibility: A metataxonomic analysis. *Antibiotics* **2021**, *10*, 268. [CrossRef]
8. Nirwati, H.; Sinanjung, K.; Fahrunissa, F.; Wijaya, F.; Napitupulu, S.; Hati, V.P.; Hakim, M.S.; Meliala, A.; Aman, A.T.; Nuryastuti, T. Biofilm formation and antibiotic resistance of Klebsiella pneumoniae isolated from clinical samples in a tertiary care hospital, Klaten, Indonesia. *BMC Proc.* **2019**, *13*, 20. [CrossRef]
9. Bagińska, N.; Cieślik, M.; Górski, A.; Jończyk-Matysiak, E. The Role of Antibiotic Resistant A. baumannii in the Pathogenesis of Urinary Tract Infection and the Potential of Its Treatment with the Use of Bacteriophage Therapy. *Antibiotics* **2021**, *10*, 281. [CrossRef]
10. Muthukrishnan, L. Multidrug resistant tuberculosis–Diagnostic challenges and its conquering by nanotechnology approach–An overview. *Chem. Biol. Interact.* **2021**, *337*, 109397. [CrossRef]
11. Vassallo, A.; Silletti, M.F.; Faraone, I.; Milella, L. Nanoparticulate antibiotic systems as antibacterial agents and antibiotic delivery platforms to fight infections. *J. Nanomater.* **2020**, *2020*, 6905631. [CrossRef]
12. Gold, K.; Slay, B.; Knackstedt, M.; Gaharwar, A.K. Antimicrobial activity of metal and metal-oxide based nanoparticles. *Adv. Ther.* **2018**, *1*, 1700033. [CrossRef]
13. Mathur, P.; Jha, S.; Ramteke, S.; Jain, N. Pharmaceutical aspects of silver nanoparticles. *Artif. Cells Nanomed. Biotechnol.* **2018**, *46*, 115–126. [CrossRef] [PubMed]
14. Bouafia, A.; Laouini, S.E.; Ahmed, A.S.; Soldatov, A.V.; Algarni, H.; Feng Chong, K.; Ali, G.A. The Recent Progress on Silver Nanoparticles: Synthesis and Electronic Applications. *Nanomaterials* **2021**, *11*, 2318. [CrossRef] [PubMed]
15. Lee, S.H.; Jun, B.-H. Silver nanoparticles: Synthesis and application for nanomedicine. *Int. J. Mol. Sci.* **2019**, *20*, 865. [CrossRef] [PubMed]
16. Vishwakarma, K.; Upadhyay, N.; Kumar, N.; Tripathi, D.K.; Chauhan, D.K.; Sharma, S.; Sahi, S. Potential applications and avenues of nanotechnology in sustainable agriculture. In *Nanomaterials in Plants, Algae, and Microorganisms*; Elsevier: Amsterdam, The Netherlands, 2018; pp. 473–500.
17. Aragaw, B.A.; Alula, M.T.; Majoni, S.; King'ondu, C.K. *Chemical Synthesis of Silver Nanoparticles Green Synthesis of Silver Nanomaterials*; Elsevier: Amsterdam, The Netherlands, 2022; pp. 21–53.
18. Fahmy, H.M.; Mosleh, A.M.; Abd Elghany, A.; Shams-Eldin, E.; Serea, E.S.A.; Ali, S.A.; Shalan, A.E. Coated silver nanoparticles: Synthesis, cytotoxicity, and optical properties. *RSC Adv.* **2019**, *9*, 20118–20136. [CrossRef]
19. Khina, A.; Krutyakov, Y.A. Similarities and Differences in the Mechanism of Antibacterial Action of Silver Ions and Nanoparticles. *Appl. Biochem. Microbiol.* **2021**, *57*, 683–693. [CrossRef]
20. Lu, T.; Qu, Q.; Lavoie, M.; Pan, X.; Peijnenburg, W.J.; Zhou, Z.; Pan, X.; Cai, Z.; Qian, H. Insights into the transcriptional responses of a microbial community to silver nanoparticles in a freshwater microcosm. *Environ. Pollut.* **2020**, *258*, 113727. [CrossRef] [PubMed]
21. Mia, R.; Sk, M.S.; Oli, Z.B.S.; Ahmed, T.; Kabir, S.; Waqar, M.A. Functionalizing cotton fabrics through herbally synthesized nanosilver. *Clean. Eng. Technol.* **2021**, *4*, 100227. [CrossRef]
22. Saleem, H.; Zaidi, S.J.; Ismail, A.F.; Goh, P.S. Advances of nanomaterials for air pollution remediation and their impacts on the environment. *Chemosphere* **2022**, *287*, 132083. [CrossRef] [PubMed]
23. Dikshit, P.K.; Kumar, J.; Das, A.K.; Sadhu, S.; Sharma, S.; Singh, S.; Gupta, P.K.; Kim, B.S. Green synthesis of metallic nanoparticles: Applications and limitations. *Catalysts* **2021**, *11*, 902. [CrossRef]
24. Soni, V.; Raizada, P.; Singh, P.; Cuong, H.N.; Rangabhashiyam, S.; Saini, A.; Saini, R.V.; Van Le, Q.; Nadda, A.K.; Le, T.T.; et al. Sustainable and green trends in using plant extracts for the synthesis of biogenic metal nanoparticles toward environmental and pharmaceutical advances: A review. *Environ. Res.* **2021**, *202*, 111622. [CrossRef]
25. Shreyash, N.; Bajpai, S.; Khan, M.A.; Vijay, Y.; Tiwary, S.K.; Sonker, M. Green synthesis of nanoparticles and their biomedical applications: A review. *ACS Appl. Nano Mater.* **2021**, *4*, 11428–11457. [CrossRef]
26. Khan, M.; Karuppiah, P.; Alkhathlan, H.Z.; Kuniyil, M.; Khan, M.; Adil, S.F.; Shaik, M.R. Green Synthesis of Silver Nanoparticles Using Juniperus procera Extract: Their Characterization, and Biological Activity. *Crystals* **2022**, *12*, 420. [CrossRef]
27. Paiva-Santos, A.C.; Herdade, A.M.; Guerra, C.; Peixoto, D.; Pereira-Silva, M.; Zeinali, M.; Mascarenhas-Melo, F.; Paranhos, A.; Veiga, F. Plant-mediated green synthesis of metal-based nanoparticles for dermopharmaceutical and cosmetic applications. *Int. J. Pharm.* **2021**, *597*, 120311. [CrossRef]
28. Rajeswari, V.D.; Khalifa, A.S.; Elfasakhany, A.; Badruddin, I.A.; Kamangar, S.; Brindhadevi, K. Green and ecofriendly synthesis of cobalt oxide nanoparticles using *Phoenix dactylifera* L: Antimicrobial and photocatalytic activity. *Appl. Nanosci.* **2021**, *2021*, 1–9. [CrossRef]

29. Garibo, D.; Borbón-Nuñez, H.A.; de León, J.N.D.; García Mendoza, E.; Estrada, I.; Toledano-Magaña, Y.; Tiznado, H.; Ovalle-Marroquin, M.; Soto-Ramos, A.G.; Blanco, A.; et al. Green synthesis of silver nanoparticles using *Lysiloma acapulcensis* exhibit high-antimicrobial activity. *Sci. Rep.* **2020**, *10*, 12805. [CrossRef] [PubMed]
30. Abomuti, M.A.; Danish, E.Y.; Firoz, A.; Hasan, N.; Malik, M.A. Green Synthesis of Zinc Oxide Nanoparticles Using Salvia officinalis Leaf Extract and Their Photocatalytic and Antifungal Activities. *Biology* **2021**, *10*, 1075. [CrossRef]
31. Oliveira, J.L.T.M.d.; Diniz, M.d.F.M.; Lima, E.d.O.; Souza, E.L.d.; Trajano, V.N.; Santos, B.H.C. Effectiveness of *Origanum vulgare* L. and *Origanum majorana* L. essential oils in inhibiting the growth of bacterial strains isolated from the patients with conjunctivitis. *Braz. Arch. Biol. Technol.* **2009**, *52*, 45–50. [CrossRef]
32. Ravichandran, V.; Vasanthi, S.; Shalini, S.; Shah, S.A.A.; Tripathy, M.; Paliwal, N. Green synthesis, characterization, antibacterial, antioxidant and photocatalytic activity of *Parkia speciosa* leaves extract mediated silver nanoparticles. *Results Phys.* **2019**, *15*, 102565. [CrossRef]
33. Sankar, R.; Karthik, A.; Prabu, A.; Karthik, S.; Shivashangari, K.S.; Ravikumar, V. *Origanum vulgare* mediated biosynthesis of silver nanoparticles for its antibacterial and anticancer activity. *Colloids Surf. B Biointerfaces* **2013**, *108*, 80–84. [CrossRef]
34. Shaik, M.R.; Khan, M.; Kuniyil, M.; Al-Warthan, A.; Alkhathlan, H.Z.; Siddiqui, M.R.H.; Shaik, J.P.; Ahamed, A.; Mahmood, A.; Khan, M.; et al. Plant-extract-assisted green synthesis of silver nanoparticles using *Origanum vulgare* L. extract and their microbicidal activities. *Sustainability* **2018**, *10*, 913. [CrossRef]
35. Arya, G.; Kumari, R.M.; Gupta, N.; Kumar, A.; Chandra, R.; Nimesh, S. Green synthesis of silver nanoparticles using Prosopis juliflora bark extract: Reaction optimization, antimicrobial and catalytic activities. *Artif. Cells Nanomed. Biotechnol.* **2018**, *46*, 985–993. [CrossRef]
36. Chinni, S.V.; Gopinath, S.C.; Anbu, P.; Fuloria, N.K.; Fuloria, S.; Mariappan, P.; Krusnamurthy, K.; Veeranjaneya Reddy, L.; Ramachawolran, G.; Sreeramanan, S.; et al. Characterization and Antibacterial Response of Silver Nanoparticles Biosynthesized Using an Ethanolic Extract of *Coccinia indica* Leaves. *Crystals* **2021**, *11*, 97. [CrossRef]
37. Rao, B.; Tang, R.-C. Green synthesis of silver nanoparticles with antibacterial activities using aqueous Eriobotrya japonica leaf extract. Advances in natural sciences. *Nanosci. Nanotechnol.* **2017**, *8*, 015014.
38. Clinical and Laboratory Standards. *Performance Standards for Antimicrobial Disk Susceptibility Tests*; Approved Standard M2-A8; Clinical and Laboratory Standards Institute (CLSI): Wayne, PA, USA, 2003.
39. Yassin, M.T.; Mostafa, A.A.-F.; Al Askar, A.A. In Vitro Evaluation of Biological Activities and Phytochemical Analysis of Different Solvent Extracts of *Punica granatum* L. *(Pomegranate) Peels. Plants* **2021**, *10*, 2742. [CrossRef]
40. Punjabi, K.; Mehta, S.; Chavan, R.; Chitalia, V.; Deogharkar, D.; Deshpande, S. Efficiency of biosynthesized silver and zinc nanoparticles against multi-drug resistant pathogens. *Front. Microbiol.* **2018**, *9*, 2207. [CrossRef]
41. Ruttkay-Nedecky, B.; Skalickova, S.; Kepinska, M.; Cihalova, K.; Docekalova, M.; Stankova, M.; Uhlirova, D.; Fernandez, C.; Sochor, J.; Milnerowicz, H.; et al. Development of new silver nanoparticles suitable for materials with antimicrobial properties. *J. Nanosci. Nanotechnol.* **2019**, *19*, 2762–2769. [CrossRef]
42. El Khoury, E.; Abiad, M.; Kassaify, Z.G.; Patra, D. Green synthesis of curcumin conjugated nanosilver for the applications in nucleic acid sensing and anti-bacterial activity. *Colloids Surf. B Biointerfaces* **2015**, *127*, 274–280. [CrossRef]
43. Delgado-Beleño, Y.; Martínez-Núñez, C.E.; Flores-López, N.S.; Meza-Villezcas, A.; Ramírez-Rodríguez, L.P.; Britto Hurtado, R.; Flores-Acosta, M.; Cortez-Valadez, M. Characterization of Silver Nanoparticles Encapsulated Using an Ion-Exchange-Mediated Method and Their Application as Antimicrobial Agents. *J. Electron. Mater.* **2021**, *50*, 5632–5638. [CrossRef]
44. Shameli, K.; Ahmad, M.B.; Zargar, M.; Yunus, W.M.Z.W.; Rustaiyan, A.; Ibrahim, N.A. Synthesis of silver nanoparticles in montmorillonite and their antibacterial behavior. *Int. J. Nanomed.* **2011**, *6*, 581. [CrossRef] [PubMed]
45. Heinemann, M.G.; Rosa, C.H.; Rosa, G.R.; Dias, D. Biogenic synthesis of gold and silver nanoparticles used in environmental applications: A review. *Trends Environ. Anal. Chem.* **2021**, *30*, e00129. [CrossRef]
46. Masum, M.; Islam, M.; Siddiqa, M.; Ali, K.A.; Zhang, Y.; Abdallah, Y.; Ibrahim, E.; Qiu, W.; Yan, C.; Li, B. Biogenic synthesis of silver nanoparticles using *Phyllanthus emblica* fruit extract and its inhibitory action against the pathogen Acidovorax oryzae strain RS-2 of rice bacterial brown stripe. *Front. Microbiol.* **2019**, *10*, 820. [CrossRef] [PubMed]
47. Skandalis, N.; Dimopoulou, A.; Georgopoulou, A.; Gallios, N.; Papadopoulos, D.; Tsipas, D.; Theologidis, I.; Michailidis, N.; Chatzinikolaidou, M. The effect of silver nanoparticles size, produced using plant extract from Arbutus unedo, on their antibacterial efficacy. *Nanomaterials* **2017**, *7*, 178. [CrossRef] [PubMed]
48. Okaiyeto, K.; Ojemaye, M.O.; Hoppe, H.; Mabinya, L.V.; Okoh, A.I. Phytofabrication of silver/silver chloride nanoparticles using aqueous leaf extract of Oedera genistifolia: Characterization and antibacterial potential. *Molecules* **2019**, *24*, 4382. [CrossRef] [PubMed]
49. Devi, T.; Ahmaruzzaman, M. Bio-inspired sustainable and green synthesis of plasmonic Ag/AgCl nanoparticles for enhanced degradation of organic compound from aqueous phase. *Environ. Sci. Pollut. Res.* **2016**, *23*, 17702–17714. [CrossRef]
50. Devi, T.B.; Ahmaruzzaman, M.; Begum, S. A rapid, facile and green synthesis of Ag@ AgCl nanoparticles for the effective reduction of 2,4-dinitrophenyl hydrazine. *New J. Chem.* **2016**, *40*, 1497–1506. [CrossRef]
51. Sidorowicz, A.; Szymański, T.; Rybka, J.D. Photodegradation of Biohazardous Dye Brilliant Blue R Using Organometallic Silver Nanoparticles Synthesized through a Green Chemistry Method. *Biology* **2021**, *10*, 784. [CrossRef] [PubMed]

52. Femi-Adepoju, A.G.; Dada, A.O.; Otun, K.O.; Adepoju, A.O.; Fatoba, O.P. Green synthesis of silver nanoparticles using terrestrial fern (*Gleichenia Pectinata* (Willd.) C. Presl.): Characterization and antimicrobial studies. *Heliyon* **2019**, *5*, e01543. [CrossRef] [PubMed]
53. Azizian-Shermeh, O.; Valizadeh, M.; Taherizadeh, M.; Beigomi, M. Phytochemical investigation and phytosynthesis of eco-friendly stable bioactive gold and silver nanoparticles using petal extract of saffron (*Crocus sativus* L.) and study of their antimicrobial activities. *Appl. Nanosci.* **2020**, *10*, 2907–2920. [CrossRef]
54. Roy, N.; Mondal, S.; Laskar, R.A.; Basu, S.; Mandal, D.; Begum, N.A. Biogenic synthesis of Au and Ag nanoparticles by Indian propolis and its constituents. *Colloids Surf. B Biointerfaces* **2010**, *76*, 317–325. [CrossRef] [PubMed]
55. Lopes, C.; Courrol, L.C. Green synthesis of silver nanoparticles with extract of *Mimusops coriacea* and light. *J. Lumin.* **2018**, *199*, 183–187. [CrossRef]
56. Tahir, K.; Nazir, S.; Li, B.; Khan, A.U.; Khan, Z.U.H.; Ahmad, A.; Khan, F.U. An efficient photo catalytic activity of green synthesized silver nanoparticles using *Salvadora persica* stem extract. *Sep. Purif. Technol.* **2015**, *150*, 316–324. [CrossRef]
57. Preet, S.; Satsangi, N. Size controlled green synthesis of biocompatible silver nanoparticles with enhanced mosquito larvicidal activity. *J. Clust. Sci.* **2019**, *30*, 1611–1621. [CrossRef]
58. Oves, M.; Rauf, M.A.; Aslam, M.; Qari, H.A.; Sonbol, H.; Ahmad, I.; Zaman, G.S.; Saeed, M. Green synthesis of silver nanoparticles by *Conocarpus Lancifolius* plant extract and their antimicrobial and anticancer activities. *Saudi J. Biol. Sci.* **2022**, *29*, 460–471. [CrossRef] [PubMed]
59. Kohan Baghkheirati, E.; Bagherieh-Najjar, M.B.; Khandan Fadafan, H.; Abdolzadeh, A. Synthesis and antibacterial activity of stable bio-conjugated nanoparticles mediated by walnut (*Juglans regia*) green husk extract. *J. Exp. Nanosci.* **2016**, *11*, 512–517. [CrossRef]
60. Al Aboody, M.S. Silver/silver chloride (Ag/AgCl) nanoparticles synthesized from Azadirachta indica lalex and its antibiofilm activity against fluconazole resistant Candida tropicalis. *Artif. Cells Nanomed. Biotechnol.* **2019**, *47*, 2107–2113. [CrossRef]
61. Singh, H.; Du, J.; Singh, P.; Yi, T.H. Role of green silver nanoparticles synthesized from *Symphytum officinale* leaf extract in protection against UVB-induced photoaging. *J. Nanostruct. Chem.* **2018**, *8*, 359–368. [CrossRef]
62. Raja, S.; Ramesh, V.; Thivaharan, V. Green biosynthesis of silver nanoparticles using *Calliandra haematocephala* leaf extract, their antibacterial activity and hydrogen peroxide sensing capability. *Arab. J. Chem.* **2017**, *10*, 253–261. [CrossRef]
63. Malassis, L.; Dreyfus, R.; Murphy, R.J.; Hough, L.A.; Donnio, B.; Murray, C.B. One-step green synthesis of gold and silver nanoparticles with ascorbic acid and their versatile surface post-functionalization. *RSC Adv.* **2016**, *6*, 33092–33100. [CrossRef]
64. Kumar, S.; Anwer, R.; Azzi, A. Virulence Potential and Treatment Options of Multidrug-Resistant (MDR) Acinetobacter baumannii. *Microorganisms* **2021**, *9*, 2104. [CrossRef]
65. Tilahun, M.; Gedefie, A.; Bisetegn, H.; Debash, H. Emergence of High Prevalence of Extended-Spectrum Beta-Lactamase and Carbapenemase Producing Acinetobacter Species and Pseudomonas aeruginosa Among Hospitalized Patients at Dessie Comprehensive Specialized Hospital, North-East Ethiopia. *Infect. Drug Resist.* **2022**, *15*, 895–911. [CrossRef] [PubMed]
66. Motbainor, H.; Bereded, F.; Mulu, W. Multi-drug resistance of blood stream, urinary tract and surgical site nosocomial infections of Acinetobacter baumannii and Pseudomonas aeruginosa among patients hospitalized at Felegehiwot referral hospital, Northwest Ethiopia: A cross-sectional study. *BMC Infect. Dis.* **2020**, *20*, 92. [CrossRef] [PubMed]
67. Lee, C.R.; Lee, J.H.; Park, M.; Park, K.S.; Bae, I.K.; Kim, Y.B.; Cha, C.J.; Jeong, B.C.; Lee, S.H. Biology of Acinetobacter baumannii: Pathogenesis, antibiotic resistance mechanisms, and prospective treatment options. *Front. Cell. Infect. Microbiol.* **2017**, *7*, 55. [CrossRef]
68. Lima, L.M.; da Silva, B.N.M.; Barbosa, G.; Barreiro, E.J. β-lactam antibiotics: An overview from a medicinal chemistry perspective. *Eur. J. Med. Chem.* **2020**, *208*, 112829. [CrossRef] [PubMed]
69. Hakyemez, I.N.; Kucukbayrak, A.; Tas, T.; Yikilgan, A.B.; Akkaya, A.; Yasayacak, A.; Akdeniz, H. Nosocomial Acinetobacter baumannii infections and changing antibiotic resistance. *Pak. J. Med. Sci.* **2013**, *29*, 1245. [CrossRef]
70. Kaviani, R.; Pouladi, I.; Niakan, M.; Mirnejad, R. Molecular detection of Adefg efflux pump genes and their contribution to antibiotic resistance in Acinetobacter baumannii clinical isolates. *Rep. Biochem. Mol. Biol.* **2020**, *8*, 413.
71. Ahmadi, M.; Ranjbar, R.; Behzadi, P.; Mohammadian, T. Virulence factors, antibiotic resistance patterns, and molecular types of clinical isolates of Klebsiella Pneumoniae. *Expert Rev. Anti-Infect. Ther.* **2022**, *20*, 463–472. [CrossRef]
72. Parvin, M.; Ali, M.; Talukder, S.; Nahar, A.; Chowdhury, E.H.; Rahman, M.; Islam, M. Prevalence and multidrug resistance pattern of methicillin resistant *S. aureus* isolated from frozen chicken meat in Bangladesh. *Microorganisms* **2021**, *9*, 636. [CrossRef]
73. Zhang, W.; Hao, Z.; Wang, Y.; Cao, X.; Logue, C.M.; Wang, B.; Yang, J.; Shen, J.; Wu, C. Molecular characterization of methicillin-resistant Staphylococcus aureus strains from pet animals and veterinary staff in China. *Vet. J.* **2011**, *190*, e125–e129. [CrossRef]
74. Sharma, M.; Jha, B.; Bhatt, C.P. Prevalence of Methicillin Resistant Staphylococcus aureus Nasal Colonizers among Basic Science MBBS and BDS Students of Kathmandu Medical College. *JNMA J. Nepal Med. Assoc.* **2021**, *59*, 19. [CrossRef]
75. Hussein, E.A.M.; Mohammad, A.A.-H.; Harraz, F.A.; Ahsan, M.F. Biologically synthesized silver nanoparticles for enhancing tetracycline activity against *staphylococcus aureus* and *klebsiella pneumoniae*. *Braz. Arch. Biol. Technol.* **2019**, *62*. [CrossRef]
76. Ansari, M.A.; Alzohairy, M.A. One-pot facile green synthesis of silver nanoparticles using seed extract of Phoenix dactylifera and their bactericidal potential against MRSA. *Evid. Based Complement. Altern.* **2018**, *2018*, 1860280. [CrossRef] [PubMed]
77. Peiris, M.K.; Gunasekara, C.P.; Jayaweera, P.M.; Arachchi, N.D.; Fernando, N. Biosynthesized silver nanoparticles: Are they effective antimicrobials? *Memórias Do Inst. Oswaldo Cruz.* **2017**, *112*, 537–543. [CrossRef] [PubMed]

78. Wright, T.; Vlok, M.; Shapira, T.; Olmstead, A.D.; Jean, F.; Wolf, M.O. Photodynamic and Contact Killing Polymeric Fabric Coating for Bacteria and SARS-CoV-2. *ACS Appl. Mater. Interfaces* **2022**, *14*, 49–56. [CrossRef] [PubMed]
79. Qamer, S.; Romli, M.H.; Che-Hamzah, F.; Misni, N.; Joseph, N.; Al-Haj, N.A.; Amin-Nordin, S. Systematic Review on Biosynthesis of Silver Nanoparticles and Antibacterial Activities: Application and Theoretical Perspectives. *Molecules* **2021**, *26*, 5057. [CrossRef]
80. Tang, S.; Zheng, J. Antibacterial activity of silver nanoparticles: Structural effects. *Adv. Healthc. Mater.* **2018**, *7*, 1701503. [CrossRef] [PubMed]
81. Santos, R.S.; Figueiredo, C.; Azevedo, N.F.; Braeckmans, K.; De Smedt, S.C. Nanomaterials and molecular transporters to overcome the bacterial envelope barrier: Towards advanced delivery of antibiotics. *Adv. Drug Deliv. Rev.* **2018**, *136*, 28–48. [CrossRef]
82. Hamad, A.; Khashan, K.S.; Hadi, A. Silver nanoparticles and silver ions as potential antibacterial agents. *J. Inorg. Organomet. Polym. Mater.* **2020**, *30*, 4811–4828. [CrossRef]
83. Singh, P.; Garg, A.; Pandit, S.; Mokkapati, V.; Mijakovic, I. Antimicrobial effects of biogenic nanoparticles. *Nanomaterials* **2018**, *8*, 1009. [CrossRef]
84. Makvandi, P.; Wang, C.y.; Zare, E.N.; Borzacchiello, A.; Niu, L.N.; Tay, F.R. Metal-based nanomaterials in biomedical applications: Antimicrobial activity and cytotoxicity aspects. *Adv. Funct. Mater.* **2020**, *30*, 1910021. [CrossRef]
85. Sharma, D.; Gulati, S.S.; Sharma, N.; Chaudhary, A. Sustainable synthesis of silver nanoparticles using various biological sources and waste materials: A review. *Emergent Mater.* **2021**, *2021*, 1–30. [CrossRef]
86. Uddin, I.; Parimi, D.S.; Bollu, T.K.; Bhatt, C.S.; Suresh, A.K. Silver Nanoparticles as Potent Multidrug-Resistant Incorporants in Biomedicine. In *Emerging Modalities in Mitigation of Antimicrobial Resistance*; Springer: Cham, Switzerland, 2022; pp. 475–488.
87. Mortazavi-Derazkola, S.; Yousefinia, A.; Naghizadeh, A.; Lashkari, S.; Hosseinzadeh, M. Green synthesis and characterization of silver nanoparticles using Elaeagnus angustifolia bark extract and study of Its antibacterial effect. *J. Polym. Environ.* **2021**, *29*, 3539–3547. [CrossRef]
88. Yun'an Qing, L.C.; Li, R.; Liu, G.; Zhang, Y.; Tang, X.; Wang, J.; Liu, H.; Qin, Y. Potential antibacterial mechanism of silver nanoparticles and the optimization of orthopedic implants by advanced modification technologies. *Int. J. Nanomed.* **2018**, *13*, 3311. [CrossRef] [PubMed]